CFD study of an air–water flow inside helically coiled pipes

Marco Colombo [1], Antonio Cammi*, Gaël Raymond Guédon, Fabio Inzoli, Marco Enrico Ricotti

Department of Energy, Politecnico di Milano, Via Lambruschini 4, 20156 Milano, Italy

Received 10 October 2014
Received in revised form
13 June 2015
Accepted 18 July 2015
Available online 8 August 2015

1. Introduction

Different nuclear reactor projects of Generation III+ and Generation IV are expected to adopt helically coiled pipes in their Steam Generators (SGs). Helical pipes provide a substantial improvement in heat and mass transfer rates and a significant enhancement of the critical heat flux during boiling and evaporation. To the higher heat transfer rates contributes the geometrical arrangement, which combines the positive features of a local cross-flow distribution with the global counter-flow along the exchanger tube (Bejan and Kraus, 2003). Helical geometry allows also handling of high temperatures and extreme temperature differentials without high induced stresses. In addition, helical pipes guarantee a compact design of the SG, reducing the required floor space (Cinotti et al., 2002). The above features improve the general efficiency of the SG, moving forward towards the goals of improved safety, performance and cost established by the nuclear community for future reactor projects.

Helical tubes are normally used in different industrial fields (Naphon and Wongwises, 2006). They have been previously adopted for the SG of more than one nuclear reactor, although mainly for prototypes or special applications. Nevertheless, issues still exist in the understanding of some complex thermal hydraulic mechanisms activated by the centrifugal force field introduced by

* Corresponding author.
E-*mail address:* antonio.cammi@polimi.it (A. Cammi).
[1] Present address: Institute of Particle Science and Engineering, School of Chemical and Process Engineering, University of Leeds, Leeds LS2 9JT, United Kingdom.

the geometry. Obviously, the complexity is further amplified by the presence of a two-phase flow. In the past, the lack of a full understanding has been solved with the adoption of conservative safety limits that guarantee safety operation despite limiting the optimal exploitation of the plant. Nowadays, overcome those limitations is made possible by the more and more powerful computational resources available for the optimization of the design and the improvement of the safety evaluations (Bousbia-Salah and D'Auria, 2007).

Recently, two-phase Computational Fluid Dynamics (CFD) has been increasingly applied in the nuclear field, as a promising way to extend simulation capabilities of many nuclear reactor thermal hydraulic issues. A Writing Group of the OECD-NEA has identified a list of nuclear reactor safety issues in which the use of two-phase CFD can provide a real benefit. Moreover, the various modeling options were identified and some first Best Practice Guidelines has been proposed (Bestion, 2012). In particular, promising is the coupling of CFD codes to best estimate system codes, adopted for safety analysis and transient thermal hydraulic calculations, as RELAP5 or TRACE (Aumiller et al., 2002; Bertolotto et al., 2009). The coupling between the codes limits the application of the more computationally expensive CFD to those areas where three dimensional flow effects and mixing phenomena are important, avoiding at the same time the modeling of the entire geometry (Anderson et al., 2008).

The capabilities of two-phase CFD can support the study of the secondary motion and the three dimensional effects that characterize the flow inside helical pipes. However, publications available on the subject are rather limited. Vashisth and Nigam (2009) simulated laminar two-phase flow in coiled ducts using the Volume of Fluid (VOF) model to study the radial asymmetry of the velocity field. A good agreement with literature experimental data is obtained. Jo et al. (2009) investigated the two-phase flow heat transfer in the helical tubes of a pressurised water reactor SG using the CFX code. They reported the formation of a liquid film on the outer portion of the tube and a good agreement with average void fraction experimental data. Jayakumar et al. (2010) presented a CFD analysis for the heat transfer of an air–water two-phase mixture flowing through a helically coiled heat exchanger, identifying the effect of different geometrical parameters. Validation against experiments is provided for the frictional pressure drop and the heat transfer coefficient. Rahimi et al. (2011) studied an air–water two-phase flow with CFD and population balance modeling (PBM) for bubble size distribution, which resulted more appropriate to capture the main flow features. Chandratilleke et al. (2012) studied flow boiling in curved pipes with a non-equilibrium model based on the Eulerian–Eulerian approach, obtaining a satisfactory agreement with experiments. In spite of the limited number of CFD studies available to date, over the years helically coiled pipes have been the subject of numerous experimental studies (Owhadi et al., 1968; Akagawa et al., 1971; Unal, 1978; Czop et al., 1994; Xin et al., 1997; Zhao et al., 2003; Santini et al., 2008; Chung et al., 2013, 2014).

In this paper, CFD is applied to the simulation of the two-phase flow inside a helically coiled duct. The ANSYS FLUENT (2011) code is selected for the simulations, with the air–water flow described through the Eulerian–Eulerian model. The capability of an accurate quantitative estimation of important physical quantities such as the frictional pressure drop and the void fraction is evaluated, with an extended validation over a wider range of conditions with respect to previous works on the subject. At the same time, the simulations are used to characterize the effect of the centrifugal force field on the two-phase flow field and the phase distribution. A relatively simple model is adopted, with the aim to limit at the same time the required computational effort. The fundamental step for a confident utilization of the numerical model is the assessment of its accuracy with experimental data. With the aim to extend the analysis to a steam–water flow in the near future, the analysis is started with the air–water flow for the larger availability of the experimental data required for the validation. Actually, for an important parameter as the void fraction, experimental data are limited to the air–water case. In particular, the simulation results are compared with experimental data of both the frictional pressure drop and the void fraction from the work of Akagawa et al. (1971). Through comparison with experiments, the capability of the model to characterize the two-phase flow inside the pipe and predict the frictional pressure drop and the void fraction is evaluated. Usually, these quantities are evaluated with empirical correlations, which are often unavoidably related to the experimental database used for their development. On the contrary, CFD could be capable of a high accuracy without being limited to a particular geometry or a narrow range of operating conditions.

2. Experimental data

A comprehensive research on air–water two-phase flow inside helically coiled pipes was published by Akagawa et al. (1971). In the paper, the authors study through experiments the flow pattern inside helical pipes and provide experimental measure-ments of both the void fraction and the frictional pressure drop. Two different helices were used, with the same tube diameter d equal to 9.93 mm and coil diameter of 0.109 m and 0.225 m, for a d/D ratio respectively of 0.091 and 0.044. The water superficial velocity j_w ranges between 0.35 m/s and 1.16 m/s, while the gas superficial velocity j_a within 0 m/s and 5 m/s. In particular, for each one of the four fixed values of the liquid flow rate, the air flow rate is gradually increased starting from a very low value. The void fraction measurements are shown in Fig. 1. The frictional pressure drop data are shown for both coils in Fig. 2, where the four liquid superficial velocities are distinguished. In both figures, experimental data are shown as a function of the flow quality x, expressed as the ratio between the air flow rate and the total flow rate. Flow quality is also used in the following sections of the paper to characterize the simulated flow conditions. In this paper, three sets of data from Akagawa et al. were considered for the assessment of the numerical results. For the 0.109 m diameter coil,

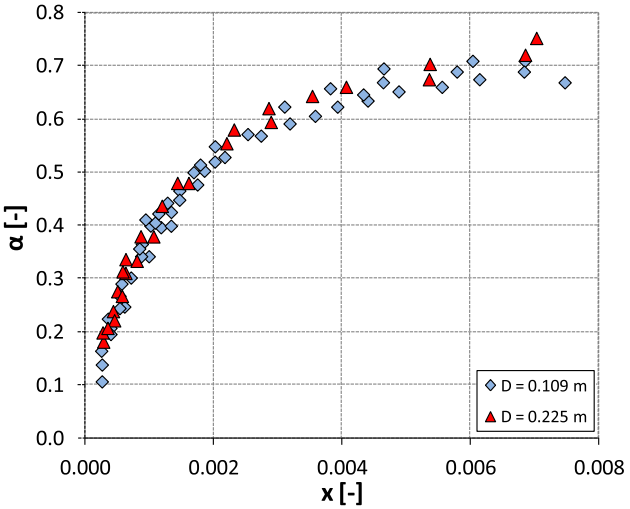

Fig. 1. Void fraction experimental data from the work of Akagawa et al. (1971). The data are related to both the helices tested by the authors (coil diameter D = 0.109 m and D = 0.225 m respectively).

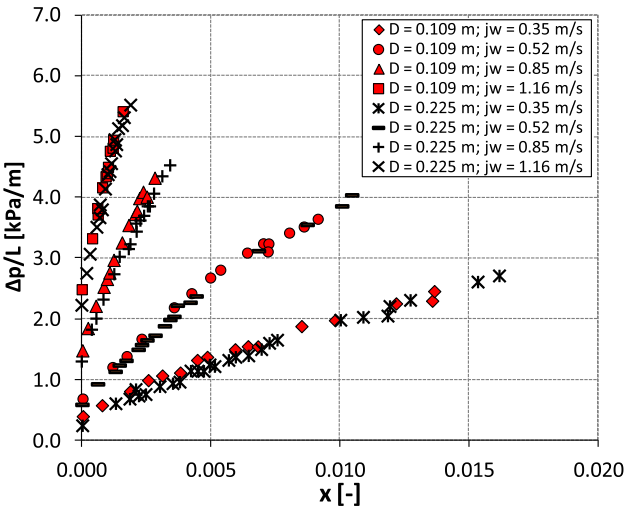

Fig. 2. Frictional pressure drop experimental data from the work of Akagawa et al. (1971). The data are related to both the helices tested by the authors (coil diameter $D = 0.109$ m and $D = 0.225$ m respectively).

the two datasets at $j_w = 0.85$ m/s and 1.16 m/s were chosen to simulate different liquid superficial velocities. A third dataset at $j_w = 0.35$ m/s was added for the 0.225 m diameter coil to extend the validation to a different coil diameter.

3. Numerical model

Numerical simulations were performed with the finite-volume ANSYS FLUENT 14.0 (2011) code. The description of a multiphase flow is a very complex subject, since the flow pattern and the distribution of the two phases might change continuously along the flow. The study of these flows is complicated by the presence of the interface and the resulting exchanges of mass, momentum and energy between the phases. In addition, since the interfacial exchanges take place in a dynamic way, multiphase flows are often not in thermal and velocity equilibrium, so that the two phases flow with different temperatures and velocities.

Between the approaches available to describe multiphase flows, the Eulerian–Eulerian model has been preferred. The Eulerian–Eulerian model describes the two phases as interpenetrating continua, where the conservation equations for each phase are based on an averaging procedure that allows both phases to coexist at any point. Since space and time averaging are applied, all the information regarding position and shape of the interface are lost. Only statistical or averaged information are available through quantities such as the void fraction, which quantifies in any point the relative weight between the phases. Being lost the detailed topology of the phases, the interfacial mass, momentum and energy exchanges need to be explicitly modeled to close the system of equations. However, with respect to other methods which track the interface position and solve interfacial phenomena and deformations to the smallest length scales without filtering (e.g., VOF), the Eulerian–Eulerian model allows preserving a large amount of computational time. In addition, in many practical situations or technological contexts there is more interest in some averaged quantities rather than in the detailed knowledge of the motion of all the particles or of the interstitial fluid. Therefore, it might be advantageous to compute directly the time evolution of these averaged quantities (Prosperetti and Tryggvason, 2007).

The adiabatic air–water mixture is simulated neglecting the phase change and the heat transfer between the phases. Therefore, the two fluids are in thermal equilibrium. The fluid properties are also considered constant and their values can be found in Table 1.

In the momentum equation, the momentum transfer between the phases is taken into account only by the drag force, whereas all the other interfacial forces are neglected. Therefore, the following set of conservation equations are solved for each phase (ANSYS FLUENT, 2011):

$$\frac{\partial}{\partial t}(\alpha_k \rho_k) + \nabla \cdot (\alpha_k \rho_k \mathbf{v}_k) = 0 \tag{1}$$

$$\frac{\partial}{\partial t}(\alpha_k \rho_k \mathbf{v}_k) + \nabla \cdot (\alpha_k \rho_k \mathbf{v}_k \mathbf{v}_k) = -\alpha_k \nabla p + \nabla \cdot \boldsymbol{T}_k + \alpha_k \rho_k \boldsymbol{g} + \sum_{p=1}^{2} \boldsymbol{R}_{pk} \tag{2}$$

In the previous equation, α_k is the volume fraction of phase k, ρ_k its density and $\mathbf{v_k}$ its velocity. p is the pressure, $\boldsymbol{T_k}$ represents the global stress tensor and R_{pk} the sum of the interfacial forces. Considering the equation for phase 1, the interaction term between the phases R_{pn} assumes the following form:

$$\boldsymbol{R}_{21} = K_{21} \cdot (\mathbf{v}_2 - \mathbf{v}_1) \tag{3}$$

In the calculation of the interaction term, it is assumed that the secondary phase is constituted by droplets or bubbles. Even if a broad range of conditions is considered in the present work, this hypothesis has been considered valid throughout all the simulations and the subject will be addressed in more details in the following sections. If phase 1 represents the continuous phase, while phase 2 the dispersed phase, the exchange coefficient K is written in the following form:

$$K_{21} = \frac{\alpha \cdot (1-\alpha) \rho_2 f}{\tau_2} \tag{4}$$

The term τ_2 represents the "particulate relaxation time", which reads:

$$\tau_2 = \frac{\rho_2 d_p^2}{18 \mu_1} \tag{5}$$

In Eq. (4), f is the drag function, calculated using the universal drag law (Kolev, 2005):

$$f = \frac{C_D Re}{24} \tag{6}$$

The drag coefficient C_D is a function of the type of two-phase flow and the flow regime. Re is the local relative velocity Reynolds number:

$$Re = \frac{\rho_1 \cdot (\mathbf{v}_1 - \mathbf{v}_2) d_p}{\mu_e} \tag{7}$$

The viscosity μ_e is the effective viscosity of the primary phase accounting for the effects of family of particles in the continuum phase. In the calculation of the momentum exchange between the phases, a crucial parameter is the diameter of the dispersed phase

Table 1
Fluid properties used in the simulation of the air–water mixture.

ρ_w [kg/m^3]	998.2
μ_w [Pa s]	0.001
ρ_a [kg/m^3]	1.225
μ_a [Pa s]	$1.79 \cdot 10^{-5}$
σ [N/m]	0.0727

d_p. Normally, its value might be determined from an empirical model, a population balance equation or from experiments. Since neither information on the value of the bubble diameter for this experiment, nor on the evolution of the bubble population in helical pipes are available, a constant fixed value of the diameter has been used, selected after a sensitivity study discussed in Section 5. The $k-\varepsilon$ turbulence model has been used to simulate the turbulence (ANSYS FLUENT, 2011). Constant inlet velocities and void fraction and outlet pressure boundary conditions were applied at the inlet and outlet boundary sections. In the near wall region, the wall boundary condition was imposed by means of the wall function and the velocity in the wall adjacent cell obeys the logarithmic law of the wall:

$$U^* = \frac{1}{\kappa}\ln(Ey^*) \tag{8}$$

In Eq. (8), $\kappa = 0.4187$ is the von Karman constant and $E = 9.793$ an empirical constant. U^* is the non-dimensional velocity and y^* the non-dimensional distance from the wall:

$$U^* = \frac{v \cdot C_\mu^{0.25} k^{0.5}}{\mu} \tag{9}$$

$$y^* = \frac{\rho \cdot C_\mu^{0.25} k^{0.5} y}{\mu} \tag{10}$$

In the previous equations, k is the turbulence kinetic energy, y the distance from the wall and $C_\mu = 0.09$. In the final part of the paper, further analyses using the code enhanced wall treatment are also presented. With the enhanced wall treatment, a two-layer approach is employed. In the fully turbulent region, the standard $k-\varepsilon$ model is resolved. Instead, the viscosity affected near wall region is resolved all the way to the viscous sublayer, using the one-equation model of Wolfhstein (1969).

The equations have been solved using the finite-volume code ANSYS FLUENT 14.0 (2011). Conservation equations have been spatially discretized on the computational grid using the second order upwind scheme for momentum and turbulence quantities and the QUICK scheme (Leonard and Mokhtari, 1990), based on a weighted average of second order upwind and central interpolations, for the void fraction. The linear system of discretized equations has then been solved using the Phase Coupled SIMPLE algorithm (ANSYS FLUENT, 2011), extension to multiphase flow of the SIMPLE algorithm (Patankar, 1980), to handle the pressure–velocity coupling. A convergence criterion of 10^{-5} was applied for velocities, volume fraction and turbulent quantities. A scheme of the simulated helical pipe is shown in Fig. 3. To reach a proper convergence of the results, simulations were run in time. The following procedure has been adopted. For every simulated condition, initially a first calculation was made with a coarser grid, to reach a developed flow condition. Outlet velocity and void fraction profiles from the first simulation are then applied as inlet conditions in successive simulations, to obtain the final simulation results. For the final set of simulations, a structured mesh including 768 elements in the pipe cross section is adopted (Fig. 4). Being the simulations made in the time domain, physical quantities are evaluated as a time average over an appropriate time interval after reaching steady-state conditions.

4. Grid sensitivity study

Considering the 0.109 m diameter coil, three different flow conditions were simulated with three meshes, characterized by an increasing number of grid points. For every grid, the number of elements in the axial direction has been determined to maintain as close as possible to 1 the aspect ratio of every hexahedral cell. The characteristics of the four grids and the conditions simulated are summarized in Table 2.

While for the average void fraction (Fig. 5) and other physical quantities mesh independent solutions were reached from the third or even the second mesh, the frictional pressure drop was considerably more influenced by the number of elements in the grid. The behavior of the frictional pressure drop per unit length as a function of the number of grid elements is also shown in Fig. 5. For the frictional pressure drop, a grid independent solution was difficult to obtain. As it will be discussed in more details in the following sections, the centrifugal force pushes the liquid phase towards the external region of the pipe. Therefore, a portion of the wall, the amount of which is function of the flow conditions, is always in contact with the liquid phase only. This water-only region is delimited by a thin separation region, after which both water and air are present, with a relative weight quantified by the local void fraction. Exact location of this separation region was particularly difficult to predict and small changes in the wall surface in contact with water triggered changes in the frictional pressure drop because air, due to its low density, has a negligible contribution. This issue may only be resolved with a finer resolution of the grid and a model able to predict the position and the geometry of the

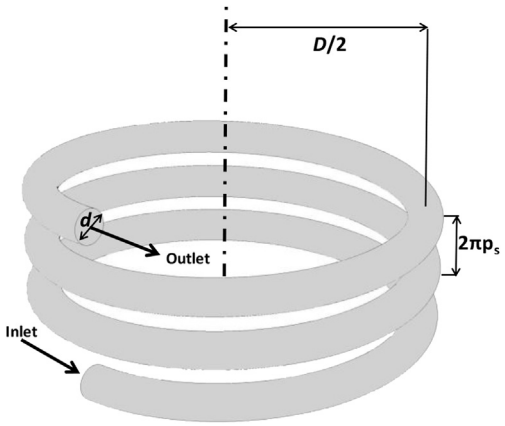

Fig. 3. Scheme of the simulated helical pipe.

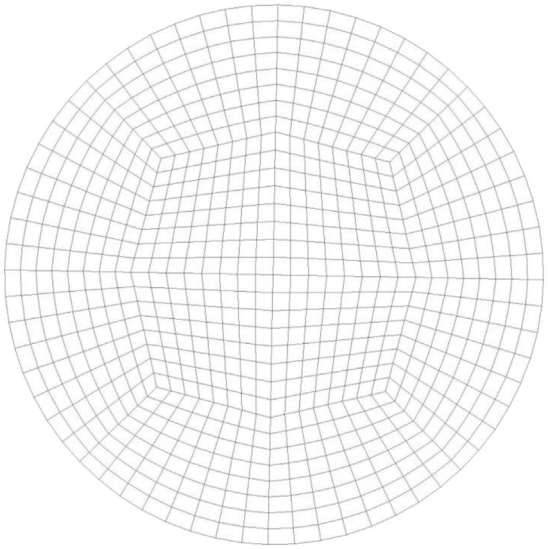

Fig. 4. Computational grid used for the simulations.

Table 2
Grid used and flow conditions simulated in the grid sensitivity study. The number of elements n in each grid is indicated as the number of elements in the tube cross section times the number of elements in the axial direction.

Mesh	n	n/V [m^{-3}]
1	192 × 100	2896
2	432 × 148	9643
3	768 × 200	23,167
4	1200 × 248	44,887

Case	j_w [m/s]	j_a [m/s]	α_{in} [−]	Re_L [−]
1	0.9	0.2	0.1	8350
2	0.8	0.6	0.2	7425
3	0.855	0.165	0.1	7935

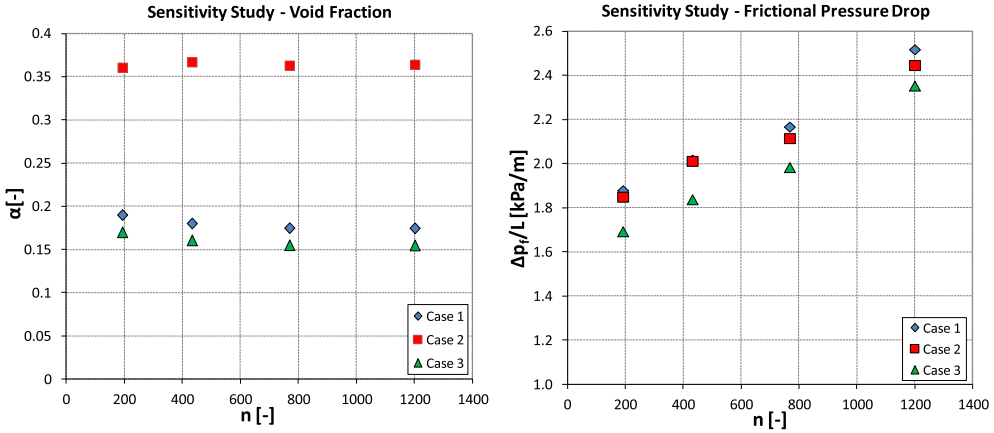

Fig. 5. Behavior of the average void fraction and the frictional pressure drop per unit length as a function of the number of cross-section elements in the computational grid.

interface. In view of the sensitivity of quantities other than the frictional pressure drop and since the finer grid already had a y^* below the suggested working range of the wall function ($30 \leq y^* \leq 300$), the mesh with 768 elements has been selected for the simulations. The change in the value of the frictional pressure drop is included in the range 5–10 % doubling the number of elements in the mesh.

5. Influence of the diameter of the dispersed phase

A large number of different parameters characterize the CFD simulation of a two-phase flow, making it a very challenging subject. Amongst them, one of the most important and sensitive parameter has been recognized in the diameter of the dispersed phase (Krepper et al., 2008, 2013; Yun et al., 2012). As stated before, the code assumes the secondary phase to form droplets or bubbles and the diameter of the dispersed phase becomes the length scale to calculate the interaction between the phases. In this view, it must be pointed out that in some conditions, as it will be shown in the following section, the influence of the centrifugal force generates a flow more similar to a separated flow than to a dispersed bubbly flow. However, bubble diameters are not available from experi-ments, neither are observation on the evolution of the bubble population. While this kind of data can be found for straight pipes (Lucas et al., 2005; Prasser et al., 2007), they are still missing for helical pipes. In particular, how the flow field produced by the centrifugal force affects the bubble population. Therefore, in absence of a more detailed experimental evidence, the air has been considered as the dispersed phase in all the simulations and a sensitivity study on the value of the diameter of the dispersed phase has been carried out.

Case 1 of the grid sensitivity study (Table 2) was simulated also with different values of the dispersed phase diameter, ranging from 0.075 mm to 0.5 mm. Increasing the value of the bubble diameter, the average value of the void fraction in the channel cross section is reduced. Consequently, the slip ratio between the phases is increased, being constant the mass flow rate of the two phases. In Figs. 6 and 7 (in these, and in all the following figures, E identifies the external and I the internal pipe wall, with respect to the pipe axis) the void fraction on the pipe cross section is shown for a dispersed phase diameter equal to 0.1 mm and 0.2 mm, respectively. Although the average value is only slightly different, as the void fraction is reduced from $\alpha = 0.173$ to $\alpha = 0.169$, higher local differences are observed. In particular, a higher separation between the two phases appears as they flow along the channel. If the diameter is increased further, the separation between the two phases is almost complete and the void fraction results very low, so the frictional pressure drop. As an example, for d_p equal to 0.5 mm, the void fraction and the frictional pressure drop are respectively 0.080 and 1.25 kPa/m, with respect to 0.173 and 2.17 kPa/m found with $d_p = 0.1$ mm. At the same time, the simulations are characterized by convergence problems, oscillations and errors in the mass balance. Reducing the value of d_p to 0.075 mm, instead, does not alter significantly the results. A further decrease, however, leads

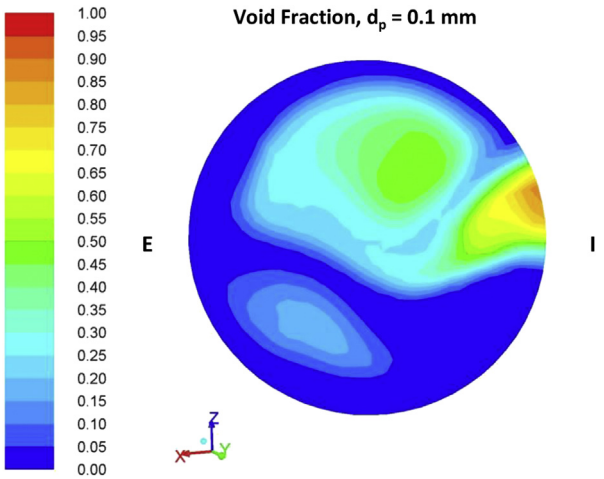

Fig. 6. Void fraction obtained for $D = 0.109$ m, $j_w = 0.9$ m/s, $j_a = 0.2$ m/s and a diameter of the dispersed phase $d_p = 0.1$ mm.

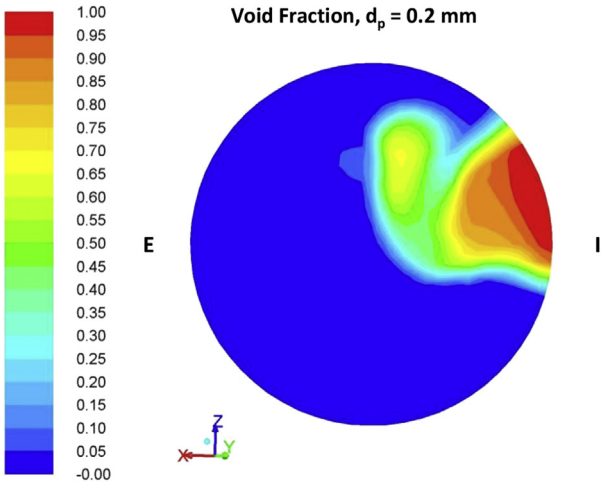

Fig. 7. Void fraction obtained for $D = 0.109$ m, $j_w = 0.9$ m/s, $j_a = 0.2$ m/s and a diameter of the dispersed phase $d_p = 0.2$ mm.

to an increase of both the void fraction and the frictional pressure drop. With a value of d_p sufficiently low, homogeneous flow conditions are reached. In other words, a higher diameter of the dispersed phase originates a weaker interaction between the two-phases, resulting in a clear separation between air and water, a higher value of the slip ratio and lower value of the void fraction. A reasonable value of the dispersed phase diameter was identified in $d_p = 0.1$ mm and maintained equal throughout all the simula-tions. The value of the diameter is lower if compared with typical air–water flow in straight pipes (Lucas et al., 2005; Prasser et al., 2007). This can be related to some deficiencies of the present model dealing with the physics of two-phase flow in helical pipes. As stated before, the presence of the centrifugal force induces some degree of separation among the phases. Therefore, the development of a more complex model, able to account for phase separation and the related modifications on the interaction between the phases, seems a possible way for further improvement.

6. Characterization of the air–water flow

Three sets of experimental conditions were considered, at $j_w = 0.85$ m/s and $j_w = 1.16$ m/s for the $D = 0.109$ m coil and at $j_w = 0.35$ m/s for the $D = 0.225$ m coil. Numerous values of air superficial velocity j_a were simulated for each condition, to study the whole range of void fraction. A summary of all the simulated conditions is provided in Table 3. In this section, the main characteristics of the air–water flow are depicted using CFD results. The simulations at $j_w = 0.85$ m/s are used as reference.

Figs. 8–10 show the void fraction profile and the phase distribution on the pipe cross section. For a very low value of the void fraction (Fig. 8), the gravitational force is dominant, since the lighter air is mainly concentrated on the upper portion of the duct. Nevertheless, a slight effect of the centrifugal force field is already observable, as the heavier water tends to occupy the external section of the pipe, whereas the air accumulates near the internal wall. In addition, a water film at the wall and a recirculation pattern of the water phase are present in the upper portion of the duct, evidence of the presence of a secondary motion. As the air flow rate is increased, so the void fraction, the effect of the centrifugal force becomes clearer (Fig. 9). The heavier water is pushed toward the outer wall of the tube, while the lighter air phase occupies the inner portion of the pipe, creating a highly unsymmetrical flow pattern in the radial direction. This phenomenon becomes more evident as the air flow rate is further increased, as shown in Fig. 10.

The relative weight between centrifugal and gravitational force fields is also influenced by the liquid superficial velocity. At the lowest value of the liquid superficial velocity ($j_w = 0.35$ m/s), the gravitational force remains dominant also for high values of void fraction and air superficial velocity (Fig. 11). On the contrary, at the highest value of the liquid superficial velocity ($j_w = 1.16$ m/s), the confinement of the water phase near the external pipe wall is even more evident (Fig. 12).

CFD results were qualitatively compared with some visual observations obtained through imaging tomography, available from the work of Murai et al. (2005). In their work, the authors observed vertical stratification and a flow dominated by gravity at low flow rates. Increasing the flow rates, the air is shifted to the center of the pipe and the water is pushed towards the external pipe wall by the centrifugal acceleration. Recirculation and secondary flows were also observed. In view of these results, qualitative agreement is found with our CFD simulations for the void fraction and the distribution of the phases. This is a preliminary confirmation of the ability of the rather simple CFD model adopted (only the drag force is considered for the interfacial momentum exchange between the phases) to reproduce the fundamental characteristics of the two-phase flow in the helical pipe. This also suggests that is the centrifugal force that mainly influences the phase distribution and the interaction between the phases.

Since the centrifugal force promotes the phase separation among the phases and, as shown in the previous figures, this phase

Table 3
CFD results in both simulated helical tubes ($D = 0.109$ m for $j_w = 0.85$ m/s and $j_w = 1.16$ m/s and $D = 0.225$ m for $j_w = 0.35$ m/s).

j_w [m/s]	j_a [m/s]	x [−]	α [−]	Δp/L [kPa/m]
0.85	0.164	0.000235	0.155	2.038
0.85	0.86	0.001227	0.438	2.579
0.85	1.25	0.001791	0.500	2.871
0.85	1.97	0.002806	0.587	3.507
0.85	2.5	0.003551	0.627	3.953
0.85	3.0	0.004269	0.657	4.308
0.85	3.5	0.004984	0.680	4.598
1.16	0.380	0.0004	0.238	3.584
1.16	0.966	0.0010	0.433	4.999
1.16	1.500	0.0016	0.516	5.751
0.35	1.013	0.0035	0.612	0.820
0.35	4.451	0.0153	0.810	2.238

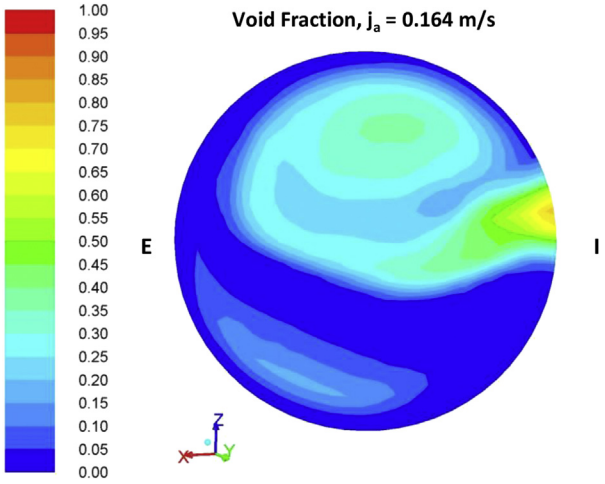

Fig. 8. Profile of the void fraction on the tube cross section for $D = 0.109$ m, $j_w = 0.85$ m/s, $j_a = 0.164$ m/s and $\alpha = 0.155$.

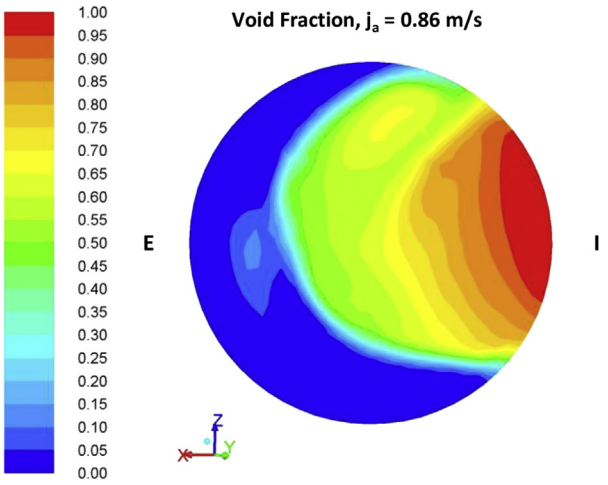

Fig. 9. Profile of the void fraction on the tube cross section for $D = 0.109$ m, $j_w = 0.85$ m/s, $j_a = 0.86$ m/s and $\alpha = 0.436$.

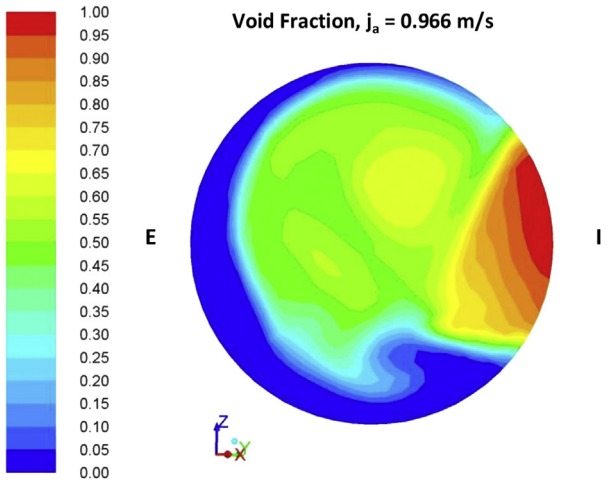

Fig. 12. Profile of the void fraction on the tube cross section for $D = 0.109$ m, $j_w = 1.16$ m/s, $j_a = 0.966$ m/s and $\alpha = 0.417$.

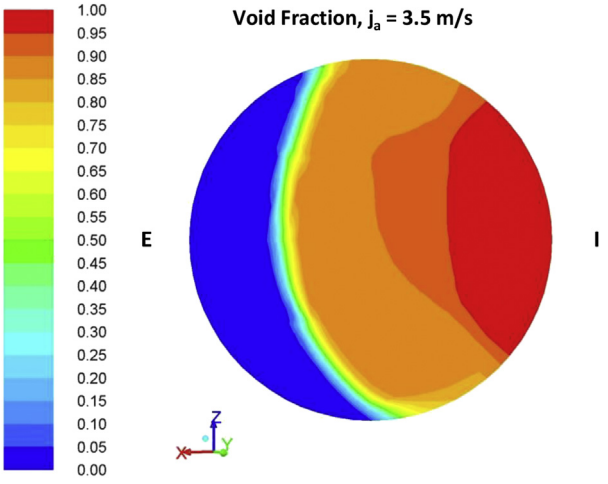

Fig. 10. Profile of the void fraction on the tube cross section for $D = 0.109$ m, $j_w = 0.85$ m/s, $j_a = 3.5$ m/s and $\alpha = 0.680$.

separation increases with the void fraction, the velocity field reflects the particular phase distribution. The air, being the fluid with the lower density, flows with a higher velocity. In addition, the relative velocity between air and water is increased due to the high separation between them. As a consequence, the maximum of the velocity is shifted near the internal wall of the pipe, where the air accumulates under the effect of the centrifugal force field. On the opposite, the outer portion of the pipe becomes a low velocity region, being occupied by the water. This phenomenon becomes more and more evident as the air flow is gradually increased. In Fig. 13, the velocity field is shown for $j_a = 1.25$ m/s.

As in single-phase flow, the centrifugal field generates a secondary motion on the channel cross-section in the form of counter rotating vortices. Fig. 14 illustrates this secondary motion. Two well defined, counter rotating vortices appear in the water region close to the external wall, together with other recirculation structures located in the maximum velocity region.

7. Comparison with experiments

All the simulation results are presented in Table 3. A first comparison with the experimental data is shown in Fig. 15 for the void

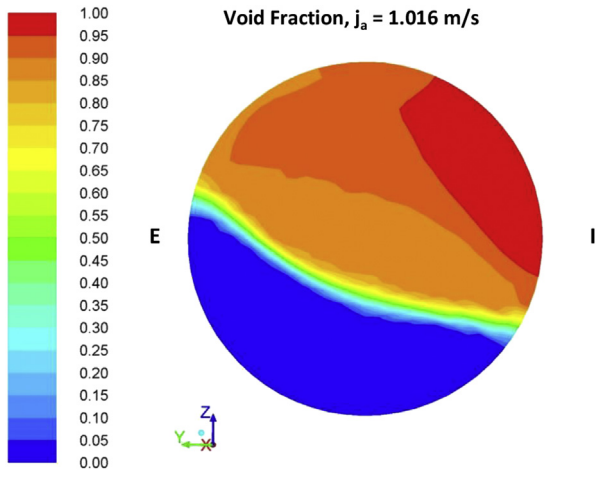

Fig. 11. Profile of the void fraction on the tube cross section for $D = 0.225$ m, $j_w = 0.85$ m/s, $j_a = 1.016$ m/s and $\alpha = 0.612$.

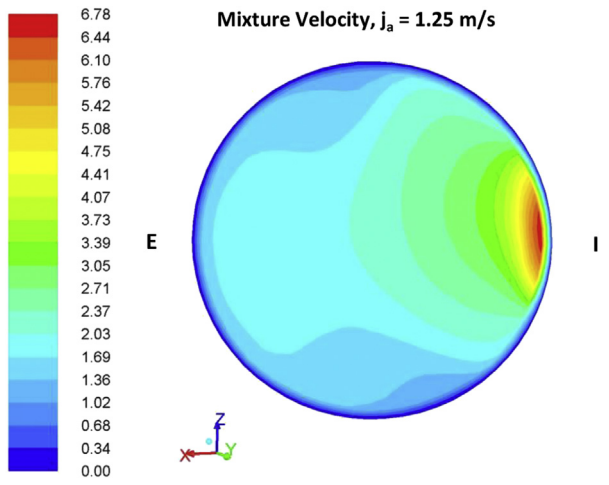

Fig. 13. Profile of the mixture velocity on the tube cross section for $D = 0.109$ m, $j_w = 0.85$ m/s, $j_a = 1.25$ m/s and $\alpha = 0.497$.

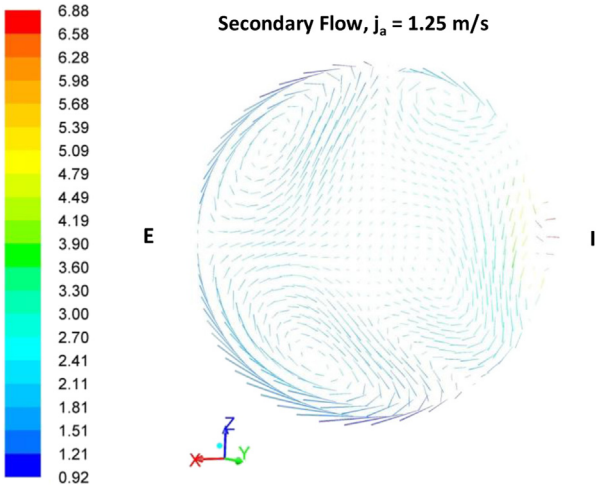

Fig. 14. Secondary flow on the tube cross section for $D = 0.109$ m, $j_w = 0.85$ m/s, $j_a = 1.25$ m/s and $\alpha = 0.497$.

fraction. Mean absolute percentage error has been used to quantify the accuracy of the simulations:

$$err(\%) = \frac{1}{N}\sum_{i=1}^{N}\frac{\left|x_{pred} - x_{exp}\right|}{x_{exp}}\cdot 100\% \qquad (11)$$

The general agreement is good and the mean absolute percentage error is about 4.5% (Table 4). In more details, the largest errors are found for the two lowest void fractions that are underestimated of more than 10%. In particular, the lowest is underestimated of more than 15%. Nevertheless, the absolute error remains very small and equal to about 0.03, being very small also the void fraction. At the same time, the higher error suggests a more complex behavior of the phase distribution at low flow quality. Therefore, a dedicated model of the drag force could be required to improve the accuracy of the simulations. The results of the previous section, indicating an interaction between the phases dominated by the centrifugal force, remain valid for higher void fraction, where the results are rather good. In particular, neglecting the points at $\alpha < 0.25$, the percentage error is reduced to 2.5%, that can be considered inside the experimental uncertainty.

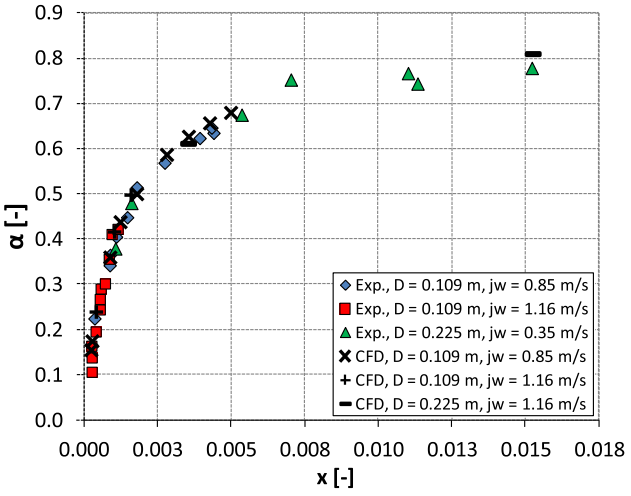

Fig. 15. Comparison between the experimental data and the CFD results for the void fraction in all the simulated conditions.

Table 4
Summary of the accuracy of the CFD simulations.

Conditions	α [%]	Δp/L [%]
D = 0.109 m, j_w = 0.85 m/s	4.5%	15.2%
D = 0.109 m, j_w = 1.16 m/s	4.8%	6.3%
D = 0.109 m, j_w = 0.35 m/s	2.0%	13.0%
Global	4.55%	12.3%

For the frictional pressure drop, the comparison is shown in Fig. 16. For the data at $j_w = 0.85$ m/s, the accuracy of the numerical results is high at low flow quality, but a systematic underestimation emerges starting from the medium flow quality. The mean absolute percentage error is about 15%, with maximum deviations included in the range ±20%. For the data at $j_w = 1.16$ m/s, the mean error is equal to 6.3%, whereas it is about 13% for the data at $j_w = 0.35$ m/s. On the whole, a mean absolute percentage error of 12.3% is found for the frictional pressure drop (Table 4). Actually, the results can be considered satisfactory, as the errors are not significantly higher with respect to the best literature correlations, when applied on their original databases. In Fig. 16, the simulation results are compared to the correlations of Akagawa et al. (1971), which shows a great accuracy as expected. In addition, also the correlation from Xin et al. (1997), obtained from air–water data in helical coils, is added for comparison. Accuracy is high for the $D =$ 0.109 m diameter coil, whereas larger errors are found for the $D =$ 0.225 m coil. Coil diameter is a critical parameter for an accurate prediction of frictional pressure drop and empirical correlations validity is often limited by the range of parameters of the experiments used for their derivation. For CFD results instead, the differences from the experimental data are almost comparable changing the flow conditions and the geometry of the coil and using the same simulation parameters.

Since the diameter of the dispersed phase has been identified as a critical parameter, some simulations ($D = 0.109$ m, $j_w = 0.85$ m/s) were repeated with a lower value of d_p. No differences were found for the void fraction, so results are shown in Fig. 17 only for the frictional pressure drop. They are compared with the experimental data and the previous simulations. At low flow quality, no significant differences are found. At medium–high flow qualities, a higher value of the frictional pressure drop is generally obtained, closer to the experimental data. The percentage error becomes 8.2% from the 15.2% obtained with the higher value of the dispersed phase diameter. Although it is possible to further improve the simulation results with a fine tuning of the diameter of the dispersed phase, the above is out of the scope of this work, seeming also more related to a case by case scenario. Actually, the main objective is to demonstrate the possibility to estimate with a satisfactory degree of accuracy the void fraction and the frictional pressure drop in a wide range of conditions. As a consequence, no more work has been done to improve the results with a further tuning of the dispersed phase diameter.

7.1. *Effect of the wall treatment*

Finally, also the influence on the results of the treatment of the near wall region has been examined. To the aim, the enhanced wall treatment of the ANSYS FLUENT code has been adopted. The enhanced wall treatment considers a two layer model in which the viscosity affected near wall region is resolved all the way to the viscous sub-layer (ANSYS FLUENT, 2011). Differently from wall function, no empirical formula is required to solve the region between the wall and the first grid point. First, since the enhanced wall treatment requires a sufficiently fine mesh, a new grid has been developed, introducing an exponentially-based refinement of

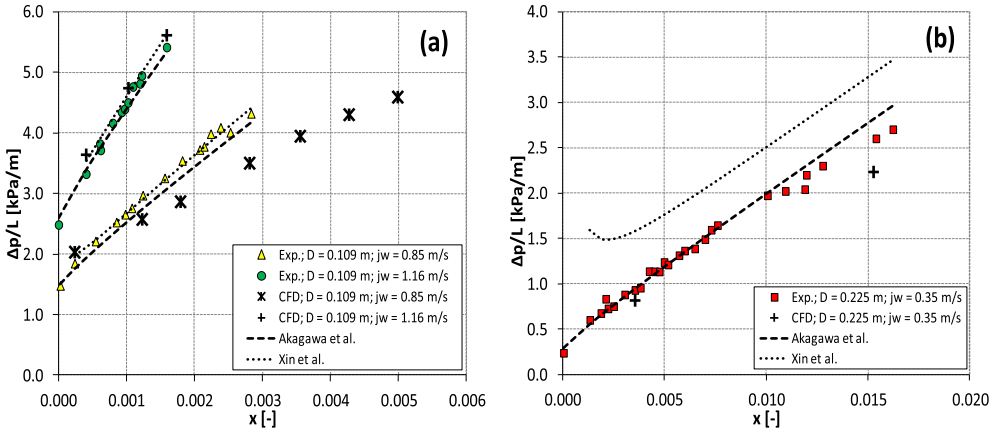

Fig. 16. Comparison between the experimental data, CFD results and correlations by Akagawa et al. (1971) and Xin et al. (1997) for the frictional pressure drop. (a) $D = 0.109$ m, $j_w = 0.85$ m/s and $j_w = 1.16$ m/s. (b) $D = 0.225$ m and $j_w = 0.35$ m/s.

the boundary layer in the mesh of Fig. 4. The new grid, composed by 1024 cells in the cross section, is shown in Fig. 18. The same experimental points used in the previous section to quantify the effect of the dispersed phase diameter have been again simulated. Numerical results are resumed in Table 5.

The presence of the boundary layer should allow a better definition of the phase distribution in the cross section of the pipe, in particular for the liquid film at the wall. Fig. 19 show a comparison between the same experimental conditions simulated with the enhanced wall treatment and the wall function. For the major part, the results are unchanged. Instead, in the region occupied by the air phase, a liquid film at the wall is present when the enhanced wall treatment is enabled. Actually, the enhanced wall treatment seems to allow a better definition of the wall region. In particular, the liquid film covers the majority of the wall and only the internal portion is excluded.

From a quantitative point of view, the average cross section values of the void fraction are unchanged with respect to previ-ous results. The frictional pressure drop is well predicted until the medium values of the void fraction. However, it is signifi-cantly overestimated at high void fraction (Fig. 20). With the use of an even finer mesh with a reduced dimension of the last cell

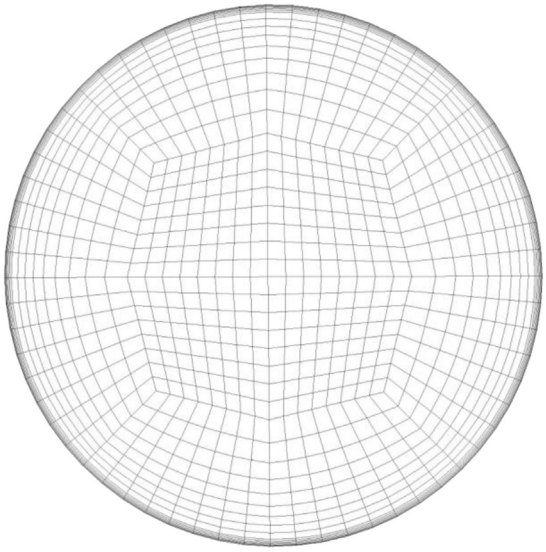

Fig. 18. Computational grid developed for the simulations with the enhanced wall treatment.

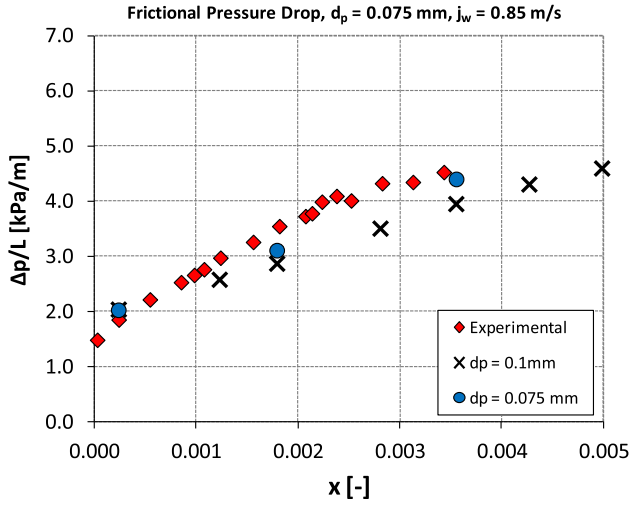

Fig. 17. Comparison between the CFD results ($D = 0.109$ m and $j_w = 0.85$ m/s) and the experimental data for different values of the dispersed phase diameter d_p.

near the wall, a slight improvement is obtained but, nevertheless, the frictional pressure drop remains overestimated (Fig. 20). Even if the use of the enhanced wall treatment seems to improve the ability to detect the presence of the liquid film at the wall, the higher errors observed in the frictional pressure drop demonstrate at the same time the limitations of the present model. In particular, the detailed description of the liquid film and the phase separation at the boundary of the film are difficult to predict with the averaged Eulerian–Eulerian two-fluid model. Therefore, the overestimation of the frictional pressure drop seems related to a predicted excessive amount of liquid in contact with the wall.

Table 5
Results of the simulation with the enhanced wall treatment.

j_w [m/s]	j_a [m/s]	x [−]	α [−]	Δp/L [kPa/m]
0.856	0.161	0.0002	0.151	2.055
0.857	1.254	0.0018	0.501	3.671
0.860	2.486	0.0035	0.634	5.913

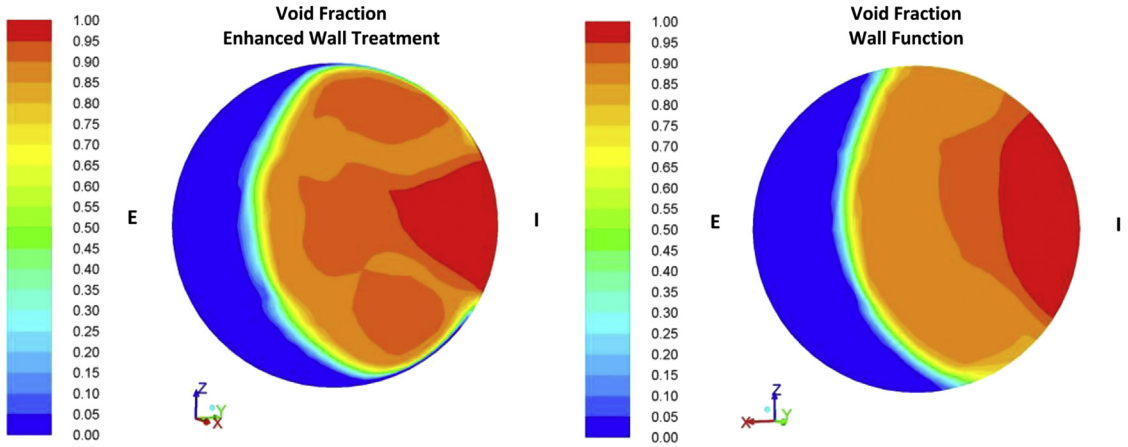

Fig. 19. Profile of the void fraction on the tube cross section obtained using for the near wall region the enhanced wall treatment and the wall function respectively ($D = 0.109$ m, $j_w = 0.85$ m/s, $j_a = 2.5$ m/s).

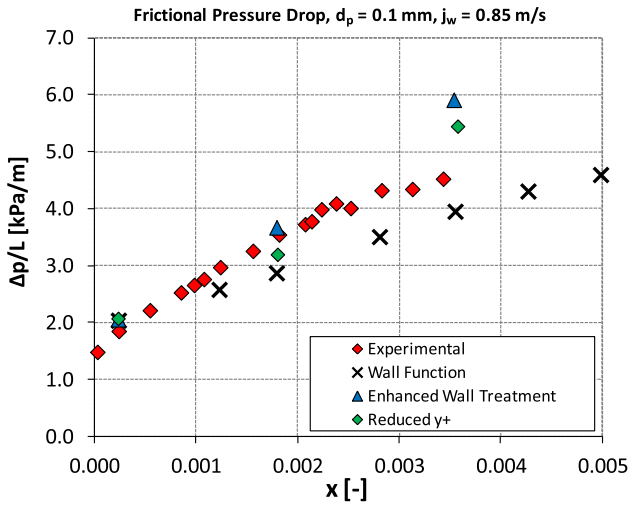

Fig. 20. Comparison between CFD frictional pressure drop results obtained with the enhanced wall treatment and the wall function.

8. Conclusions

In this paper, a CFD study of two-phase air–water flow inside helically coiled pipes has been carried out. The ANSYS FLUENT code has been used, describing the two component mixture through the Eulerian–Eulerian model. An adiabatic mixture has been considered, neglecting heat transfer between the phases. In addition, in the relatively simple model adopted, interphase momentum transfer has been considered entirely due to the drag force and all other interphase forces have been neglected.

Simulations results highlighted the effect on the two-phase flow of the centrifugal force field introduced by the geometry. The water, being the heavier phase, is pushed by the centrifugal force toward the outer pipe wall, whereas air accumulates in the inner region of the pipe. As a consequence, the maximum of the mixture velocity is found near the inner pipe wall, as the air flows much faster than the water, having a considerably lower density. Similarly to single-phase flow, flow recirculation and vortices characterize the flow field. Some agreement was obtained with the experimental observations of the phase distribution provided in the work of Murai et al. (2005). The value of the dispersed phase diameter was found to be particularly significant for the accuracy of the simulations and its value has been carefully selected, being unavailable information from the experiments.

Simulation results were validated against the experimental measurements of Akagawa et al. (1971) for the average void fraction and the frictional pressure drop. Void fraction predictions were in good agreement with experiments, with a mean absolute per-centage error of about 4.5%. A satisfactory estimation of the fric-tional pressure drop was also obtained, with a mean absolute percentage error of 12.3%. In this regard, accurate estimations can be obtained with the relatively simple model adopted, which limit at the same time the computational costs of the simulations. Therefore, the CFD model could be considered a reliable and, with respect to other CFD approaches, computationally efficient predictive tool for void fraction and frictional pressure drop, which are relevant in the design of industrial components employing helically coiled pipes. In addition, accuracy was not significantly influenced by flow conditions and coil geometry, which always limit the range of applicability of empirical correlations. At the same time, some drawbacks of the present model were also identified. Two-phase flows in helical pipes are characterized by separation and stratification among the phases because of the presence of the gravitational and the centrifugal force fields, which may potentially limit the applicability of the present model, based on a dispersed secondary phase. Therefore, to improve the capabilities of the present model, a more advanced formulation, able to account for phase separation and the presence of large interfaces, seems necessary. At the same time, the addition of other relevant terms to momentum interphase transfer would be beneficial. These improvements, even if at the expense of the computational cost, would further improve the prediction of the internal flow pattern and the quantitative estimation of the frictional pressure drop.

Nomenclature

C_D	drag coefficient [−]
D	coil diameter [m]
d	tube diameter [m]
d_p	diameter of the dispersed phase [m]
f	drag function [−]
g	gravitational acceleration [m/s^2]
j	superficial velocity [m/s]
K	momentum interphase exchange coefficient [kg/m^3 s]
k	turbulence kinetic energy [m^2/s^2]
L	length [m]

n number of elements in the mesh [−]
p pressure [Pa]
p_s helical pipe pitch per radiant [m/rad]
R momentum interphase source term [kg/m^2 s^2]
Re Reynolds number [−]
T stress tensor [Pa]
t time [s]
U^* non-dimensional velocity [−]
V volume [m^3]
v velocity [m/s]
x flow quality [−]
y wall distance [m]
y^* non-dimensional wall distance [−]

Greek symbols

α void fraction [−]
μ viscosity [Pa s]
ρ density [kg/m^3]
σ surface tension [N/m]
τ relaxation time [s]

Subscripts

a air
e effective
in inlet
w water

References

Akagawa, B.K., Sakaguchi, T., Ueda, M., 1971. Study on a gas-liquid two-phase flow in helically coiled tubes. JSME Int. J. B 14 (72), 564−571.

Anderson, N., Hassan, Y., Schultz, R., 2008. Analysis of the hot gas flow in the outlet plenum of the very high temperature reactor using coupled RELAP5-3D system code and a CFD code. Nucl. Eng. Des. 238, 274−279.

ANSYS Fluent 14.0 User Guide, 2011.

Aumiller, D.L., Tomlinson, E.T., Weaver, W.L., 2002. An integrated RELAP5-3D and multiphase CFD code system utilizing a semi-implicit coupling technique. Nucl. Eng. Des. 216, 77−87.

Bejan, A., Kraus, A.D., 2003. Heat Transfer Handbook. Wiley.

Bertolotto, D., Manera, A., Frey, S., Prasser, H.M., Chawla, R., 2009. Single-phase mixing studies by means of a directly coupled CFD/system code tool. Ann. Nucl. Energy 36, 310−316.

Bestion, D., 2012. Applicability of two-phase CFD to nuclear reactor thermal-hydraulics and elaboration of best practice Guidelines. Nucl. Eng. Des. 253, 311−321.

Bousbia-Salah, A., D'Auria, F., 2007. Use of coupled code technique for best estimate safety analysis of nuclear power plants. Prog. Nucl. Energy 49, 1−13. Chandratilleke, T.T., Nadim, N., Narayanaswamy, R., 2012. An investigation of flow boiling with secondary flow interaction in curved pipes. In: ECI 8th International Conference on Boiling and Condensation Heat Transfer, Lausanne, Switzerland, 3−7 June.

Chung, Y.J., Kim, H.J., Chung, B.D., Lee, W.J., Kim, M.H., 2013. Thermo-hydraulic characteristics of the helically coiled tube and the condensate heat exchanger for SMART. Ann. Nucl. Energy 55, 49−54.

Chung, Y.J., Bae, K.H., Kim, K.K., Lee, W.J., 2014. Boiling heat transfer and dryout in helically coiled tubes under different pressure conditions. Ann. Nucl. Energy 71, 298−303.

Cinotti, L., Bruzzone, M., Meda, N., Corsini, G., Lombardi, C., Ricotti, M., Conway, L., 2002. Steam generator of the international reactor innovative and secure. In: Proceedings of the 10th Conference on Nuclear Engineering (ICONE 10), Arlington, VA, USA, 14−18 April.

Czop, V., Barbier, D., Dong, S., 1994. Pressure drop, void fraction and shear stress measurements in an adiabatic two-phase flow in a coiled tube. Nucl. Eng. Des. 149, 323−333.

Jayakumar, J.S., Mahajani, S.M., Mandal, J.C., Iyer, K.N., Vijayan, P.K., 2010. Thermal hydraulic characteristics of air-water two-phase flows in helical pipes. Chem. Eng. Res. Des. 88, 501−512.

Jo, J.C., Kim, W.S., Choi, C.Y., Lee, Y.K., 2009. Numerical simulation of subcooled flow boiling heat transfer in helical tubes. J. Pressure Vessel-Trans. ASME 131.

Kolev, N.I., 2005. Multiphase Flow Dynamics 2: Thermal and Mechanical Interactions, second ed. Springer, Berlin, Germany.

Krepper, E., Lucas, D., Frank, T., Prasser, H.M., Zwart, P.J., 2008. The inhomogeneous MUSIG model for the simulation of polydispersed flows. Nucl. Eng. Des. 238, 1690−1702.

Krepper, E., Rzehak, R., Lifante, C., Frank, T., 2013. CFD for subcooled flow boiling: coupling wall boiling and population balance models. Nucl. Eng. Des. 255, 330−346.

Leonard, B.P., Mokhtari, S., 1990. Ultra-sharp Nonoscillatory Convection Schemes for High-speed Steady Multidimensional Flow. NASA Lewis Research Center. NASATM1−2568.

Lucas, D., Krepper, E., Prasser, H.M., 2005. Development of co-current air-water flow in a vertical pipe. Int. J. Multiphase Flow 31, 1304−1328.

Murai, Y., Oiwa, H., Sasaki, T., Kondou, K., Yoshikawa, S., Yamamoto, F., 2005. Backlight imaging tomography for gas-liquid two-phase flow in a helically coiled tube. Meas. Sci. Technol. 16, 1459−1468.

Naphon, P., Wongwises, S., 2006. A review of flow and heat transfer characteristics in curved tubes. Renew. Sustain. Energy Rev. 10, 463−490.

Owhadi, A., Bell, K.J., Crain Jr., B., 1968. Forced convection boiling inside helically-coiled tubes. Int. J. Heat Mass Transfer 11, 1779−1793.

Patankar, S.V., 1980. Numerical Heat Transfer and Fluid Flow. Hemisphere, Washington, DC, USA.

Prasser, H.M., Beyer, M., Carl, H., Gregor, S., Lucas, D., Pietruske, H., Schutz, P., Weiss, F.P., 2007. Evolution of the structure of a gas-liquid two-phase flow in a large vertical pipe. Nucl. Eng. Des. 237, 1848−1861.

Prosperetti, A., Tryggvason, G., 2007. Computational Methods for Multiphase Flow. Cambridge University Press, Cambridge, UK.

Rahimi, M.R., Askari, A., Ghanbari, M., 2011. Simulation of two-phase flow and heat transfer in helical pipes. In: 2nd International Conference on Chemistry and Chemical Engineering IPCBEE, Singapore.

Santini, L., Cioncolini, A., Lombardi, C., Ricotti, M.E., 2008. Two-phase pressure drops in a helically coiled steam generator. Int. J. Heat Mass Transfer 51, 4926−4939.

Unal, H.C., 1978. Determination of void fraction, incipient point of boiling, and initial point of net vapor generation in sodium-heated helically coiled steam generator tubes. Trans. ASME, J. Heat Transfer 100, 268−274.

Vashisth, S., Nigam, K.D.P., 2009. Prediction of flow profiles and interfacial phenomena for two-phase flow in coiled tubes. Chem. Eng. Process 48, 452−463.

Wolfhstein, M., 1969. The velocity and temperature distribution of one-dimensional flow with turbulence augmentation and pressure gradient. Int. J. Heat Mass Transfer 12, 301−318.

Xin, R.C., Awwad, A., Dong, Z.F., Ebadian, M.A., 1997. An experimental study of single-phase and two-phase flow pressure drop in annular helicoidal pipes. Int. J. Heat Fluid Flow 18, 482−488.

Yun, B.J., Splawski, A., Lo, S., Song, C.H., 2012. Prediction of a subcooled boiling flow with advanced two-phase flow models. Nucl. Eng. Des. 253, 351−359.

Zhao, L., Guo, L., Bai, B., Hou, Y., Zhang, X., 2003. Convective boiling heat transfer and two-phase flow characteristics inside a small horizontal helically coiled tubing once through steam generator. Int. J. Heat Mass Transfer 46, 4779−4788.